Electronic Supplementary Material (ESI) for ChemComm.
This journal is © The Royal Society of Chemistry 2023

Electronic Supplementary Information

Narrow-band deep-blue MRTADF-type organic afterglow

Guangming Wang,[#a] Shuhui Ding,[#a] Jiuyang Li,[#a] Zi Ye,[a] Wen Xia,[a] Xuefeng Chen,[a] and Kaka Zhang*[a]

[a] Key Laboratory of Synthetic and Self-Assembly Chemistry for Organic Functional Molecules, Shanghai Institute of Organic Chemistry, University of Chinese Academy of Sciences, Chinese Academy of Sciences, 345 Lingling Road, Shanghai 200032, People's Republic of China.

*Correspondence: zhangkaka@sioc.ac.cn.

#equal contribution.

Table of Contents

Materials

Preparation of 1-matrix samples

Preparation of 1-PMMA emulsions

Physical measurements and instrumentation

Text S1. About the T_1 level of PhB matrix.

Text S2. About the small FWHM of compound 1 system.

Figure S1. HPLC profile of compound **1**.

Figure S2. (A) The prompt fluorescence decay profiles of compound **1** in dichloromethane (DCM) solution excited at 365 nm and monitored at 406 nm. (B) Steady-state emission spectra of compound **1** in DCM solution at different concentrations. The emission maxima and band shape of the steady-state emission spectra show insignificant change by varying the concentration from 10^{-5} to 10^{-7} mol/L.

Figure S3. Photographs of compound **1** in solid state (A, crystal; B, powder) and solution state (C, dichloromethane solution) under 365 nm UV light and after removal of the UV light.

Figure S4. (A) UV-vis absorption spectra of PhB film. (B) Room-temperature steady-state emission spectra (black line) and delayed emission spectra (red line, 1 ms decay) of PhB matrices only excited at 365 nm. The inset shows the photographs of PhB matrices under 365 nm irradiation and after the remove of 365 nm UV lamp. PhB matrices don't show room-temperature afterglow (Fig S3 and Fig S4). The emission spectra of **1**-PhB-0.001% (Fig 1c) and **1**-PhB-0.01% (Fig S6) samples are very similar to those of compound **1** in dichloromethane solution (Fig 1b). Therefore, the afterglow behaviours in **1**-PhB samples can be exclusively attributed to compound **1** rather than PhB matrix.

Figure S5. CIE coordinate of **1**-PhB-0.001% sample.

Figure S6. (A) Room-temperature steady-state and delayed emission spectra (1 ms delay) and (B) emission decay (monitored at 406 nm) of **1**-PhB-0.01% solid sample excited at 365 nm.

Figure S7. Photographs of **1**-matrix-0.001% samples under 365 nm UV light and after removal of the UV light. Various organic matrices (such as benzoic acid, boric acid and 4-methoxybenzophenone) have been also tried to accommodate luminescent dopants to obtain afterglow materials and their chemical structure have been also displayed, but the resultant 1-matrix samples show weak room-temperature afterglow and the afterglow colors is cyan rather than deep-blue.

Figure S8. (A) HOMO/LUMO energy levels of PhB matrix calculated at TPSSh/6-31G(d,p) level. (B) Iso-surface maps of electron-hole density difference of PhB matrix's excited states calculated at TPSSh/6-31G(d,p) level, where blue and green iso-surfaces correspond to hole and electron distributions, respectively.

Figure S9. (A) Iso-surface maps of electron-hole density difference of compound **1**'s singlet and triplet excited states calculated at TPSSh/6-31G(d,p) level, where blue and green iso-surfaces correspond to hole and electron distributions, respectively, and spin-orbit coupling matrix element (SOCME) values. (B) HOMO/LUMO energy levels of compound **1** calculated at TPSSh/6-31G(d,p) level.

Figure S10. (A) Normalized UV-vis absorption spectra of compound **1** in DCM. (B) Excitation spectra of **1**-PhB-0.001% sample excited at 365 nm. The match between UV-vis and excitation spectra suggest that the luminescent property originates from compound **1** rather than impurity.

Figure S11. Afterglow photographs of **1**-PhB-0.001% sample at 77 K.

Figure S12. The emission decay curve (excited at 365 nm and monitored at 406 nm) of **1**-PhB-0.001% sample at 77 K.

Figure S13. (A) Temperature-dependent emission decay curves of **1**-PhB-0.001% sample. (B) Arrhenius plot of the k_{RISC} from the triplet states to the singlet states of compound **1**. The straight line (least-squares regression) is used to determine the activation energy. In rigid crystalline PhB matrix where nonradiative decay (k_{nr}) and oxygen quenching (k_q) of triplet excited states have been largely suppressed at low temperature and also at room temperature or higher, k_{RISC} can be estimated as $k_{RISC} = 1/\tau_{DF} - k_P$, given RISC is the rate-determine step of TADF-type organic afterglow here. At 77 K, k_{RISC} would be very small, so k_P can be estimated from delayed emission lifetime at 77 K (837 ms) to be 1.2 s^{-1}. The k_{RISC} values at different temperatures can thus be obtained from the decay profile as shown in (A) and have been illustrated in (B). It should be noted that, because of the large difference in delayed fluorescence lifetimes between TADF afterglow emitter here and conventional TADF OLED emitter, here the estimation of k_{RISC} values is also different from that in conventional TADF system (Adachi and coworkers, *Nature*, **2012**, *492*, 234–238). Arrhenius plot of the k_{RISC} gives experimental ΔE_{ST} of 0.39 eV, which agrees well with that estimated from fluorescence and phosphorescence maxima (S_1 level, 3.05 eV; T_1 level, 2.67 eV; ΔE_{ST}, 0.38 eV).

Figure S14. (A-B) Power-dependent delayed fluorescence spectra (1 ms delay) of **1**-PhB-0.001% sample excited at 365 nm. It is found that the intensity of delayed fluorescence of the

afterglow materials exhibit a quasi-linear dependence on the excitation dose, which further support the TADF mechanism.

Figure S15. The prompt fluorescence decay profiles of **1**-PhB-0.001% sample excited at 365 nm and monitored at 406 nm.

Figure S16. TD-DFT calculations of compound **1** (gas), compound **1** in ethyl acetate (EA) and methyl benzoate (PhCOOMe). Ethyl acetate and methyl benzoate are used to mimic phenyl benzoate (PhB) matrix because of their structural similarity. The S_1 levels and ΔE_{ST} values of compound 1 in ethyl acetate and methyl benzoate are lower than that in gas state, which suggest the interaction between compound **1** and its environment. ΔE_{ST} values are important parameter for intersystem crossing; the decrease of ΔE_{ST} values would lead to significant enhancement of ISC, that is, the population of **1**'s triplet excited states. The calculation of dipole moments and excited state energy levels in different environments support the statement that "PhB matrices can also assist the population of dopants' triplets via dipole-dipole interactions" in the main text.

Table S1. CCSD total energies of S_0 and excitation energies (S_0-S_1 and S_0-T_1) in eV of compound **1** calculated at the STEOM-DLPNO-CCSD/def2-TZVP level of theory.

Table S2. The ground state (S_0) and excited state electronic energies (S_1 and T_1) in eV of compound **1** calculated at the STEOM-DLPNO-CCSD/def2-TZVP level of theory. The zero point of the energies is set to be the S_0 energy for the S_0 geometry. The smallest S_1, T_1 and S_0 energies are underlined, which are used for the calculation of adiabatic energy difference (ΔE_{AD}) in equation (1) and (2).

Table S3. Absolute value of SOCMEs (cm^{-1}) calculated at STEOM-DLPNO-CCSD/def2-TZVP level of theory of compound **1**.

Table S4. Transition electric dipole moments (a.u) of compound **1** calculated at STEOM-DLPNO-CCSD/def2-TZVP level of theory.

Table S5. Fluorescence emission and intersystem crossing rate constants (s^{-1}) calculated fro the S_0, S_1, T_1 and T_2 geometries of compound **1**.

Table S6. Optimized S_0 geometry of compound **1** at the TPSSh/6-31+G(d,p) level of theory (Å).

Table S7. Optimized S_1 geometry of compound **1** at the TPSSh/6-31+G(d,p) level of theory (Å).

Table S8. Optimized T_1 geometry of compound **1** at the TPSSh/6-31+G(d,p) level of theory (Å).

Experimental Procedures

Materials

10-Phenylacridone (compound **1**, 98%, Leyan Company, Shanghai), phenyl benzoate (PhB, 99%, Energy Chemical), benzoic acid (99.5%, Aladdin), boric acid (99.5%, Sinopharm Chemical Reagent), 4-methoxybenzophenone (MeOBP, 98%, Adamas), methyl methacrylate (99.5%, Aladdin), potassium persulfate (99%, Innochem), Pluronic F127 (Sigma).

Preparation of 1-matrix samples

For the preparation of 1-PhB-0.001%, the purchased 10-phenylacridin-9-one (compound **1**) was first purified by recrystallization in spectroscopic grade dichloromethane/hexane. Then, 10 μL compound **1** in dichloromethane (0.1 mg/mL) and 100 mg phenyl benzoate (PhB) were added into a 3 mL sample bottle, and the mixture was heated to 80 °C. After standing at room temperature for tens of minutes, **1**-PhB-0.001% sample was obtained. Other samples using different organic matrices were prepared through similar processes.

Preparation of 1-PMMA emulsions

0.5 mg oil-soluble compound **1** was firstly dissolved in 120 μL of methyl methacrylate (MMA) and then added into a 10 mL Schlenk tube containing 3 mL 25 mg/mL Pluronic F127 aqueous solution. The mixture solution was preemulsified by sonication, after that 0.5 mL 2 mg/mL potassium persulfate (KPS, a water-soluble initiator) aqueous solution was added. After three cycles of freeze–pump–thaw–degassing procedures, the obtained liquid precursor was heated at 90 ºC for 1 h. After the polymerization, **1**-PMMA emulsions were obtained.

Physical measurements and instrumentation

UV-Vis absorption spectra were recorded on a Techcomp UV1050 UV-vis spectrophotometer. The steady-state and delayed emission spectra were collected by Hitachi FL-4700 fluorescence spectrometer equipped with chopping systems; the delayed emission spectra were obtained with a delay time of approximately 1 ms. The excited state decay profiles in millisecond to second region were collected by Hitachi FL-4700 fluorescence spectrometer equipped with chopping systems. Emission spectra were recorded using Edinburgh FLS1000 fluorescence spectrometer, Hitachi FL-7000 fluorescence spectrometer and Horiba FluoroLog-3 fluorescence spectrometer. The fluorescence decay profiles in nanosecond region were recorded by using time-correlated single photon counting technique

(TCSPC) on a Edinburgh FLS1000 fluorescence spectrometer equipped with a picosecond pulsed diode laser. Photoluminescence quantum yield was measured by a Hamamatsu absolute PL quantum yield measurement system based on a standard protocol (*Adv. Mater.* **1997**, *9*, 230). Photographs and videos were captured by HUAWEI P30 and iphone 12 cameras. Before the capture, samples were irradiated by a 365 nm UV lamp (5 W) for approximately 5 s at a distance of approximately 15 cm.

Computational methods

Kaji's method using TPSSh functional has been reported (ref. 52 in the main text) to give theoretical calculation results of MRTADF emitter consistent with experimental results, so we use TPSSh functional to study the photophysical property compound **1** in the present study. The geometries of ground state and excited states were optimized at the TPSSh/6-31+G(d,p) or TD-TPSSh/6-31+G(d,p) level of theory using the polarizable continuum model to simulate CH_2Cl_2 solvent environment. And the frequency analyses were performed at the same level of theory. No imaginary modes were obtained. All of the calculations mentioned above were performed by Gaussian 16 package.[1] Then, excited states were computed using the STEOM-DLPNO-CCSD method with def2-TZVP basis set by ORCA 5.0.3 program.[2,3] The obtained electronic structures were analyzed by Multiwfn 3.8 software.[4,5] All isosurface maps to show the hole-electron distribution were rendered by Visual Molecular Dynamics (VMD 1.9.3) software[6] based on the exported files generated by Multiwfn 3.8.

According to Fermi's Golden Rule (FGR)[7], the fluorescence ($S_1 \rightarrow S_0$) rates can be calculated as

$$k_{\mathrm{F}} = \frac{4\Delta E_{AD}(S_1 - S_0)^3}{3\epsilon_0 \hbar^4 c^3} \mu_F(S_1 \rightarrow S_0)^2 \quad \#(1)$$

where the $\Delta E_{AD}(S_1 - S_0)$ is the adiabatic energy difference between S_n and S_0, $\mu_F(S_1 \rightarrow S_0)$ is the transition dipole moment of $S_1 \rightarrow S_0$, ϵ_0 is the vacuum electric permittivity, $\hbar$ is the reduced Planck constant and c is the speed of light in vacuum.

The ISC and RISC rates were estimated by semiclassical Marcus rate expression:[8,9]

$$k_{\mathrm{ISC}}(S_m\text{-}T_n) = \frac{2\pi}{\hbar} \frac{|\langle S_m|\mathbf{H_{SO}}|T_n\rangle|^2}{\sqrt{4\pi\lambda k_B T}} exp\left(-\frac{(\lambda \pm \Delta E_{AD}(S_m\text{-}T_n))^2}{4\lambda k_B T}\right) \#(2)$$

where the $|\langle S_m|\mathbf{H_{SO}}|T_n\rangle|$ is the norm of the spin-orbit coupling matrix element, the + (-) sign is associated with k_{RISC} and k_{ISC}, ΔE_{AD} is the adiabatic energy difference between singlet

excited state (S_m) and triplet excited state (T_n), λ is the reorganization energy, T is the temperature and k_B is the Boltzmann constant.

The dipole moment of compound **1** in ground state and S_1 state have been calculated at TPSSh/6-31G(d,p) level to be 4.99 Debye and 17.36 Debye, respectively. PhB has dipole moment of 2.02 Debye in ground state also calculated at TPSSh/6-31G(d,p) level.

Text S1. About the T_1 level of PhB matrix.

PhB matrices have been frequently used in our study for dopant-matrix afterglow fabrication (*Angew. Chem. Int. Ed.* **2021**, *60*, 17138; *Chem. Commun.* **2021**, *57*, 8794; *Chem. Eng. J.* **2022**, *431*, 134197; *Sci. China Chem.* **2023**, *66*, 1120; *Nat. Commun*. **2023**, *14*, 1987). We tried many times to estimate the T_1 level of PhB matrices from their phosphorescence spectra but we didn't obtain satisfactory phosphorescence spectra possibly due to the inefficient ISC of PhB. Here we use different methods to estimate PhB's T_1 level (3.53 eV, 3.46 eV and 3.38 eV as calculated by TD-B3LYP/6-31G(d,p), TD-B3LYP/def2-TZVP(-f) and TD-TPSSh/6-31G(d,p), respectively). T_1 level of compound **1** was obtained from phosphorescence maximum to be 2.67 eV (Fig 2a). From these results, PhB should have a much higher T_1 level than compound **1**, so we reason that the statement in the main text "PhB has high T_1 level (approximately 3.4 eV estimated by TD-DFT), which can resist excited state energy transfer from dopant to matrix and subsequent afterglow quenching" is correct.

Text S2. About the small FWHM of compound 1 system.

The electron-hole iso-surface maps of **1**'s S_1 state exhibit multiple resonance feature within the acridone backbone, despite the mixing of intramolecular charge transfer character from 10-phenyl group to acridone backbone. Such S_1 states still possess MR effect and show narrow-band emission, which agree with the reported studies (*ACS Appl. Mater. Interfaces* **2019**, *11*, 13472). One may concern that the excited state relaxation of compound **1** due to the presence of the relatively flexible 10-phenyl group may cause emission spectral broadening. Acridone and 10-methylacridone don't possess such flexible 10-phenyl group. The emission spectra of acridone (λ_{em}, 400 nm; FWHM, 36 nm) and 10-methylacridone (λ_{em}, 412 nm; FWHM, 37 nm) in dichloromethane have been found to be similar to that of compound **1** (λ_{em}, 406 nm; FWHM, 35 nm). These results suggest that the presence of 10-phenyl group has insignificant influence on the FWHM value of compound **1**. According to the reported studies (*Nat. Photonics*, **2019**, *13*, 678 and others), MRTADF emitters with relatively flexible phenyl group on them can still show very small FWHM. Therefore, the small FWHM of compound **1** system should be attributed to (1) the structural rigidity of acridone backbone and (2) the multiple resonance effect.

Room-temperature delayed emission spectra (1 ms delay, excited at 365 nm) show narrow emission band at 406 nm with CIE coordinate (0.158, 0.048) and small FWHM of 38 nm (Fig 1c, Fig S5). With reference to the reported study (*Nat. Photonics*, **2019**, *13*, 678), the

slight increase of FWHM from 35 nm (in dichloromethane solution) to 38 nm (in PhB matrix) after doping into PhB should be probably caused by some non-covalent interaction between **1** and PhB.

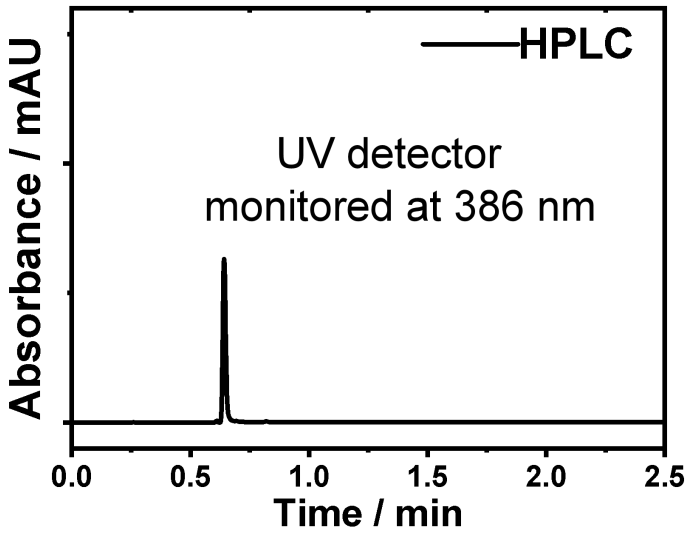

Figure S1. HPLC profile of compound **1**.

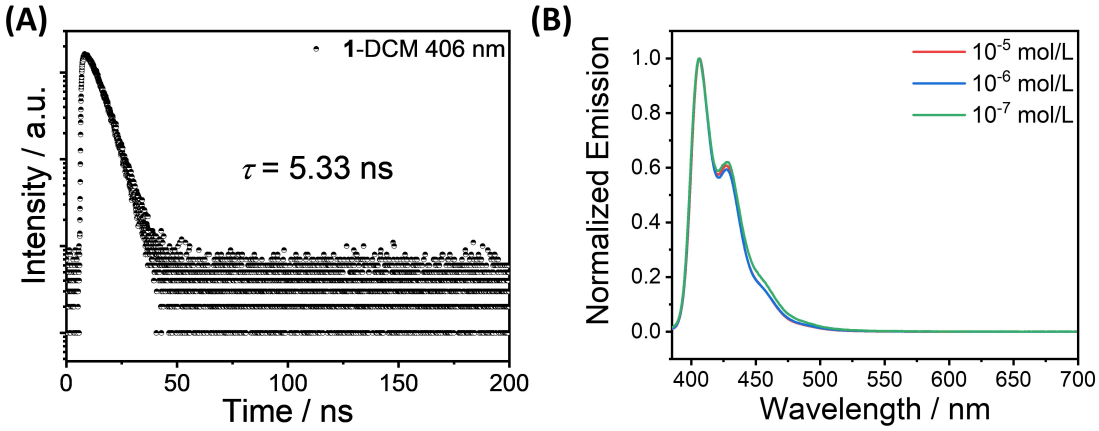

Figure S2. (A) The prompt fluorescence decay profiles of compound **1** in dichloromethane (DCM) solution excited at 365 nm and monitored at 406 nm. (B) Steady-state emission spectra of compound **1** in DCM solution at different concentrations. The emission maxima and band shape of the steady-state emission spectra show insignificant change by varying the concentration from 10^{-5} to 10^{-7} mol/L.

Figure S3. Photographs of compound **1** in solid state (A, crystal; B, powder) and solution state (C, dichloromethane solution) under 365 nm UV light and after removal of the UV light.

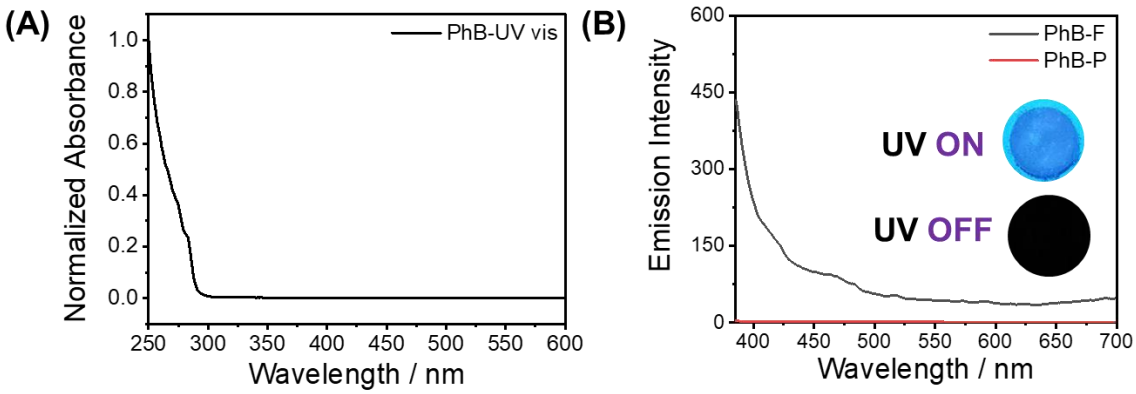

Figure S4. (A) UV-vis absorption spectra of PhB film. (B) Room-temperature steady-state emission spectra (black line) and delayed emission spectra (red line, 1 ms decay) of PhB matrices only excited at 365 nm. The inset shows the photographs of PhB matrices under 365 nm irradiation and after the remove of 365 nm UV lamp. PhB matrices don't show room-temperature afterglow (Fig S3 and Fig S4). The emission spectra of **1**-PhB-0.001% (Fig 1c) and **1**-PhB-0.01% (Fig S6) samples are very similar to those of compound **1** in dichloromethane solution (Fig 1b). Therefore, the afterglow behaviours in **1**-PhB samples can be exclusively attributed to compound **1** rather than PhB matrix.

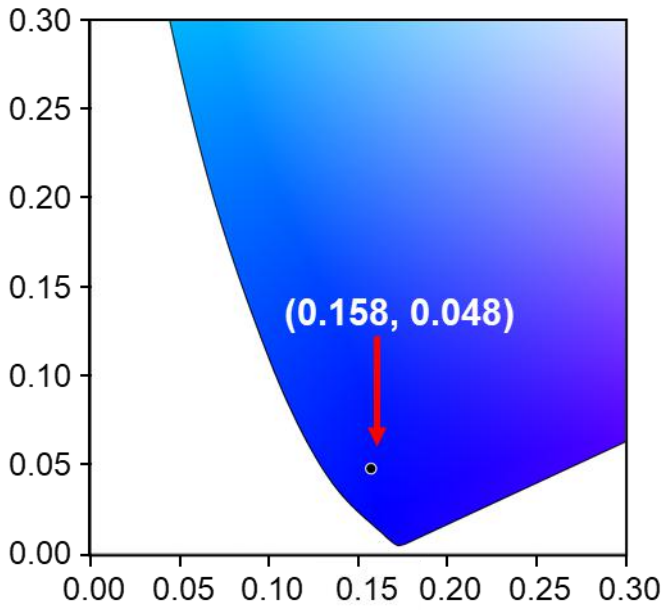

Figure S5. CIE coordinate of **1**-PhB-0.001% sample.

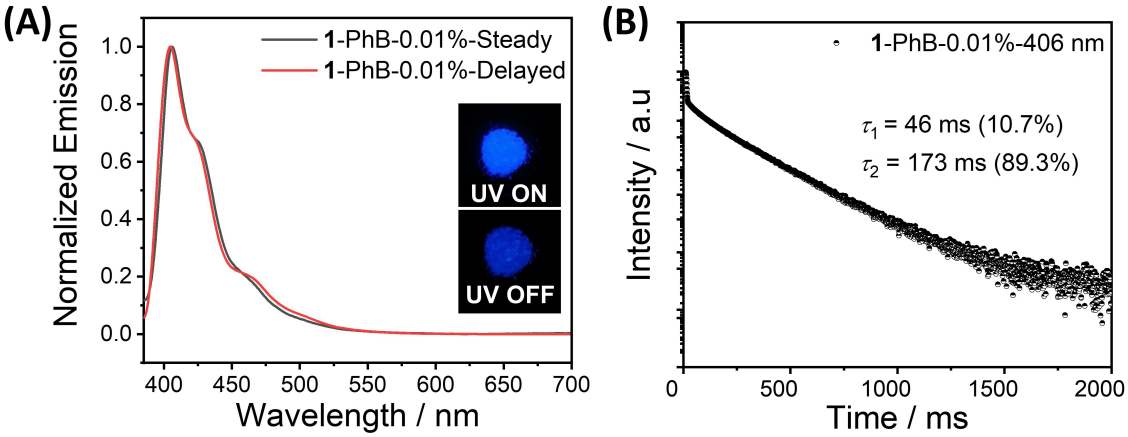

Figure S6. (A) Room-temperature steady-state and delayed emission spectra (1 ms delay) and (B) emission decay (monitored at 406 nm) of **1**-PhB-0.01% solid sample excited at 365 nm.

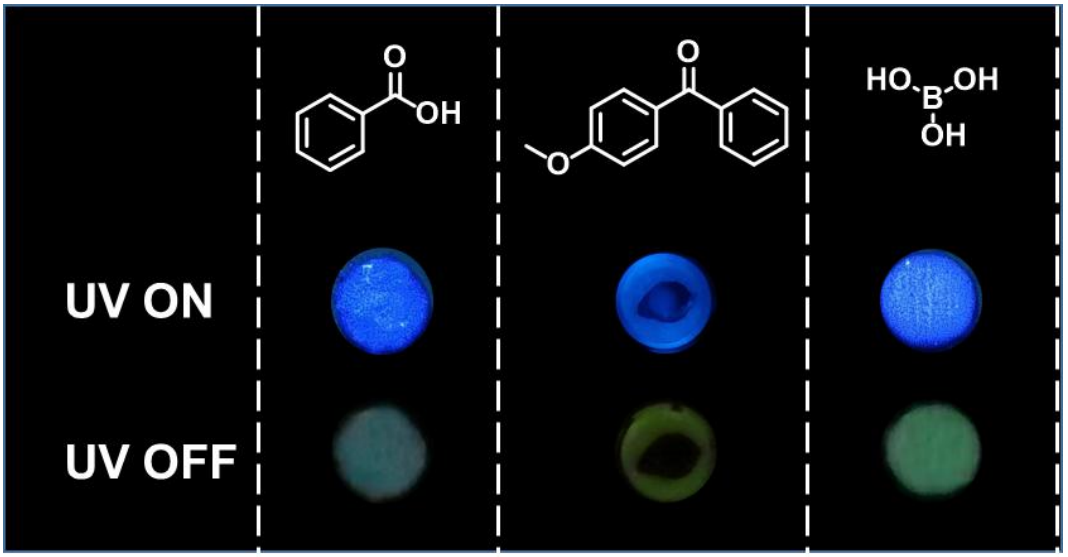

Figure S7. Photographs of **1**-matrix-0.001% samples under 365 nm UV light and after removal of the UV light. Various organic matrices (such as benzoic acid, boric acid and 4-methoxybenzophenone) have been also tried to accommodate luminescent dopants to obtain afterglow materials and their chemical structure have been also displayed, but the resultant **1**-matrix samples show weak room-temperature afterglow and the afterglow colors is cyan rather than deep-blue.

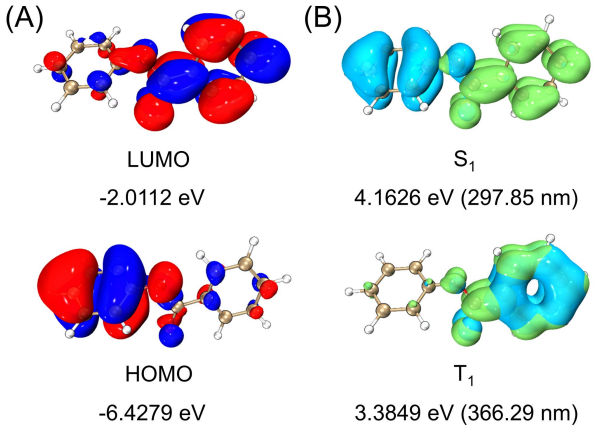

Figure S8. (A) HOMO/LUMO energy levels of PhB matrix calculated at TPSSh/6-31G(d,p) level. (B) Iso-surface maps of electron-hole density difference of PhB matrix's excited states calculated at TPSSh/6-31G(d,p) level, where blue and green iso-surfaces correspond to hole and electron distributions, respectively.

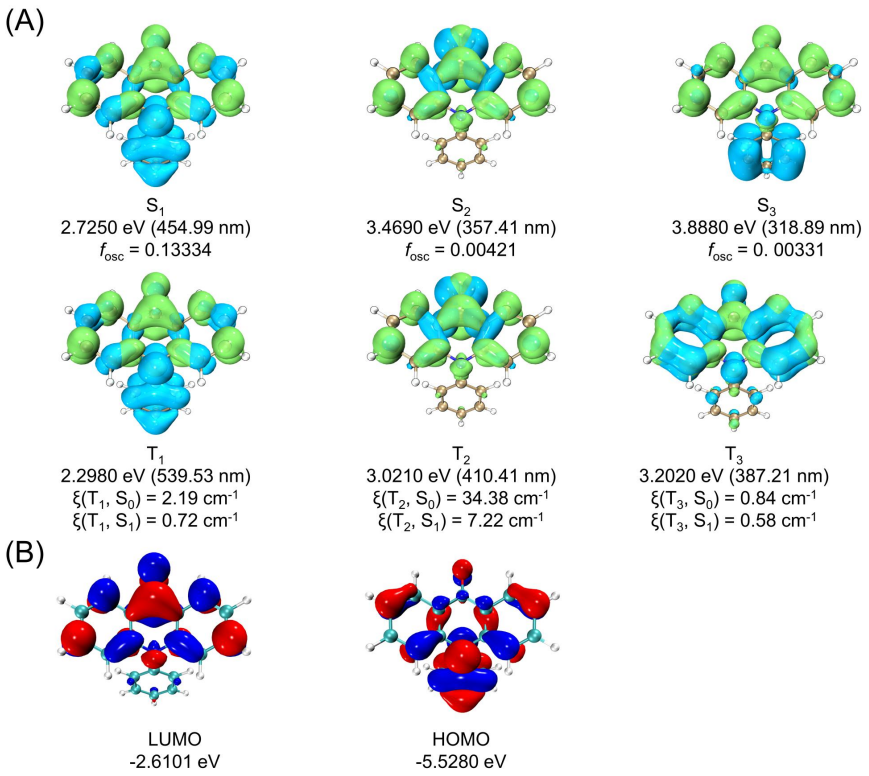

Figure S9. (A) Iso-surface maps of electron-hole density difference of compound **1**'s singlet and triplet excited states calculated at TPSSh/6-31G(d,p) level, where blue and green iso-surfaces correspond to hole and electron distributions, respectively, and spin–orbit coupling matrix element (SOCME) values. (B) HOMO/LUMO energy levels of compound **1** calculated at TPSSh/6-31G(d,p) level.

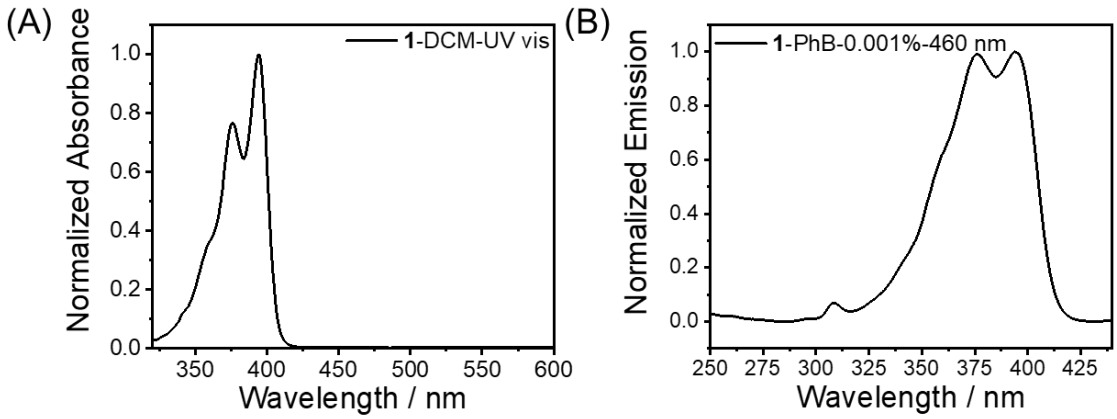

Figure S10. (A) Normalized UV-vis absorption spectra of compound **1** in DCM. (B) Excitation spectra of **1**-PhB-0.001% sample excited at 365 nm. The match between UV-vis and excitation spectra suggest that the luminescent property originates from compound **1** rather than impurity.

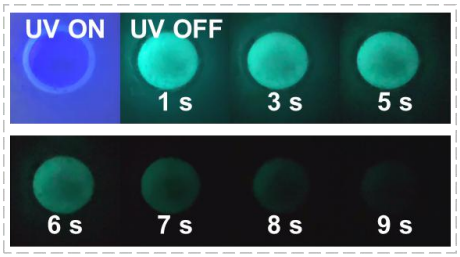

Figure S11. Afterglow photographs of **1**-PhB-0.001% sample at 77 K.

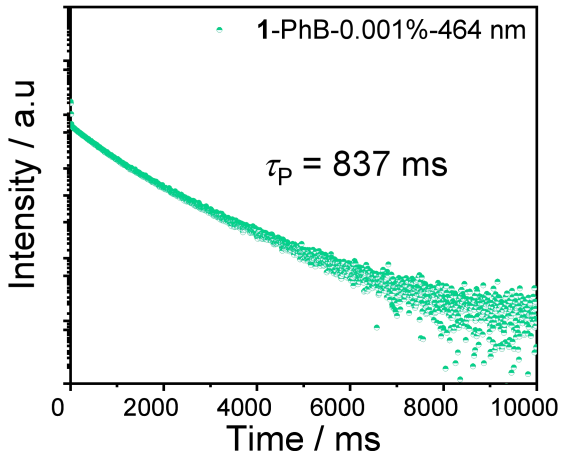

Figure S12. The emission decay curve (excited at 365 nm and monitored at 406 nm) of **1**-PhB-0.001% sample at 77 K.

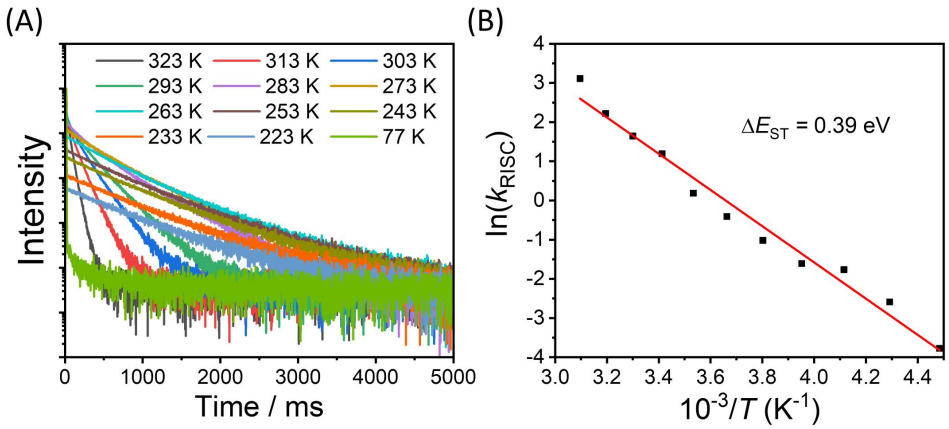

Figure S13. (A) Temperature-dependent emission decay curves of **1**-PhB-0.001% sample. (B) Arrhenius plot of the k_{RISC} from the triplet states to the singlet states of compound **1**. The straight line (least-squares regression) is used to determine the activation energy. In rigid crystalline PhB matrix where nonradiative decay (k_{nr}) and oxygen quenching (k_q) of triplet excited states have been largely suppressed at low temperature and also at room temperature or higher, k_{RISC} can be estimated as $k_{RISC} = 1/\tau_{DF} - k_P$, given RISC is the rate-determine step of TADF-type organic afterglow here. At 77 K, k_{RISC} would be very small, so k_P can be estimated from delayed emission lifetime at 77 K (837 ms) to be 1.2 s^{-1}. The k_{RISC} values at different temperatures can thus be obtained from the decay profile as shown in (A) and have been illustrated in (B). It should be noted that, because of the large difference in delayed fluorescence lifetimes between TADF afterglow emitter here and conventional TADF OLED emitter, here the estimation of k_{RISC} values is also different from that in conventional TADF system (Adachi and coworkers, *Nature*, **2012**, *492*, 234–238). Arrhenius plot of the k_{RISC} gives experimental ΔE_{ST} of 0.39 eV, which agrees well with that estimated from fluorescence and phosphorescence maxima (S_1 level, 3.05 eV; T_1 level, 2.67 eV; ΔE_{ST}, 0.38 eV).

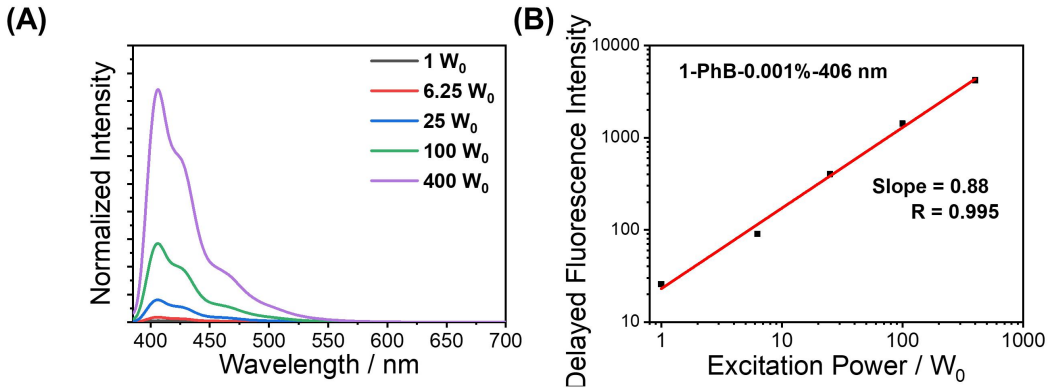

Figure S14. (A-B) Power-dependent delayed fluorescence spectra (1 ms delay) of **1**-PhB-0.001% sample excited at 365 nm. It is found that the intensity of delayed fluorescence of the afterglow materials exhibit a quasi-linear dependence on the excitation dose, which further support the TADF mechanism.

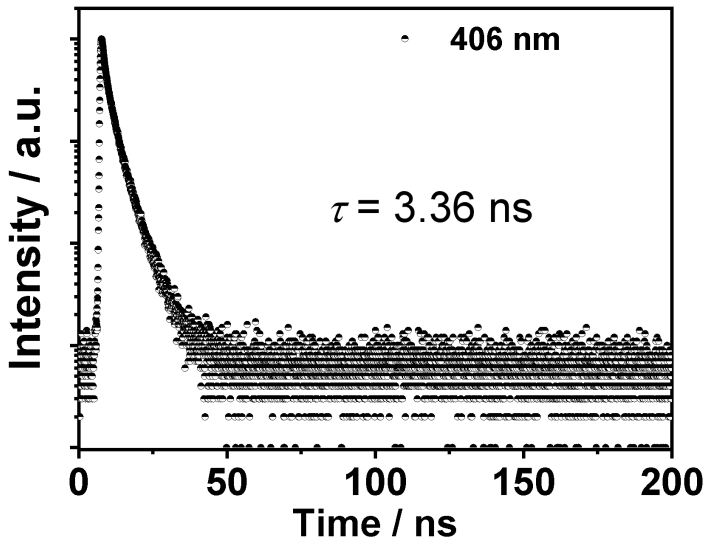

Figure S15. The prompt fluorescence decay profiles of **1**-PhB-0.001% sample excited at 365 nm and monitored at 406 nm.

(A)

Conditions	S_1 / eV	T_1 / eV	ΔE_{ST} / eV
In gas	2.8449	2.3860	0.4589
In EA	2.7785	2.3450	0.4335
In PhCOOMe	2.7693	2.3435	0.4258

(B)

	In gas	In EA	In PhCOOMe
LUMO	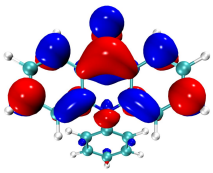 -2.4836 eV	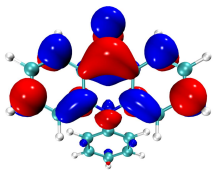 -2.4166 eV	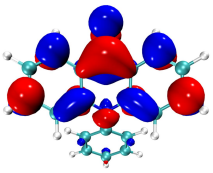 -2.4183 eV
HOMO	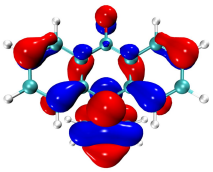 -5.4809 eV	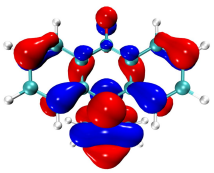 -5.3691 eV	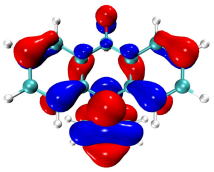 -5.3691 eV

Figure S16. TD-DFT calculations of compound **1** (gas), compound **1** in ethyl acetate (EA) and methyl benzoate (PhCOOMe). Ethyl acetate and methyl benzoate are used to mimic phenyl benzoate (PhB) matrix because of their structural similarity. The S_1 levels and ΔE_{ST} values of compound **1** in ethyl acetate and methyl benzoate are lower than that in gas state, which suggest the interaction between compound **1** and its environment. ΔE_{ST} values are important parameter for intersystem crossing; the decrease of ΔE_{ST} values would lead to significant enhancement of ISC, that is, the population of **1**'s triplet excited states. The calculation of dipole moments and excited state energy levels in different environments support the statement that "PhB matrices can also assist the population of dopants' triplets via dipole-dipole interactions" in the main text.

Table S1. CCSD total energies of S_0 and excitation energies (S_0-S_1 and S_0-T_1) in eV of compound **1** calculated at the STEOM-DLPNO-CCSD/def2-TZVP level of theory.

	S_0 geometry	S_1 geometry	T_1 geometry
S_0	-23311.60658	-23311.05682	-23311.14694
S_0-S_1	3.2368	2.4975	2.7086
S_0-T_1	2.7672	2.3173	2.3225

Table S2. The ground state (S_0) and excited state electronic energies (S_1 and T_1) in eV of compound **1** calculated at the STEOM-DLPNO-CCSD/def2-TZVP level of theory. The zero point of the energies is set to be the S_0 energy for the S_0 geometry. The smallest S_1, T_1 and S_0 energies are underlined, which are used for the calculation of adiabatic energy difference (ΔE_{AD}) in equation (1) and (2).

	S_0 geometry	S_1 geometry	T_1 geometry
S_0	**<u>0.0000</u>**	0.5498	0.4596
S_1	3.2368	**<u>3.0473</u>**	3.1682
T_1	**<u>2.7672</u>**	2.8671	2.7821

Table S3. Absolute value of SOCMEs (cm^{-1}) calculated at STEOM-DLPNO-CCSD/def2-TZVP level of theory of compound **1**.

	S_0 geometry	S_1 geometry	T_1 geometry
$\lvert\langle T_1\lvert\mathcal{H}_{SOC}\rvert S_0\rangle\rvert$	2.32	3.32	2.42
$\lvert\langle T_1\lvert\mathcal{H}_{SOC}\rvert S_1\rangle\rvert$	0.16	0.35	0.17

Table S4. Transition electric dipole moments (a.u) of compound **1** calculated at STEOM-DLPNO-CCSD/def2-TZVP level of theory.

	S_0 geometry	S_1 geometry	T_1 geometry
$S_1 - S_0$	1.5831	8.9777×10^{-1}	1.4264
$T_1 - S_0$	3.9799×10^{-4}	7.8588×10^{-4}	4.9588×10^{-4}

Table S5. Fluorescence emission and intersystem crossing rate constants (s^{-1}) calculated for the S_0, S_1, and T_1 geometries of compound **1**.

	S_0 geometry	S_1 geometry	T_1 geometry
$k_F(S_1\rightarrow S_0)$	9.47×10^{8}	3.05×10^{8}	7.69×10^{8}
$k_{ISC}(S_1\rightarrow T_1)$	2.50×10^{6}	1.19×10^{7}	2.82×10^{6}
$k_{RISC}(T_1\rightarrow S_1)$	5.86	2.80×10^{1}	6.62

Table S6. Optimized S_0 geometry of compound **1** at the TPSSh/6-31+G(d,p) level of theory (Å).

Atom	X	Y	Z
O	3.04594461	-0.00202763	1.77199928
C	2.13964328	-0.00127155	0.92535229
C	1.60218711	-1.23820151	0.32388680
C	2.34259566	-2.43260301	0.39414032
H	3.26088311	-2.42755310	0.97298337
C	1.92158328	-3.56935366	-0.28535387
H	2.50019958	-4.48597895	-0.23477615
C	0.76154878	-3.50726157	-1.07462461
H	0.45200403	-4.37152442	-1.65435662
C	0.00842158	-2.33665195	-1.14710721
H	-0.86447988	-2.29171717	-1.78864902
C	0.40083831	-1.19800575	-0.42171161
N	-0.36110245	0.00052086	-0.46278881
C	-1.74658714	0.00096968	-0.06978950
C	-2.44101262	1.20601537	0.16322232
H	-1.94369560	2.16125465	0.07007195
C	-3.78162429	1.19921986	0.55623148
H	-4.27659171	2.15146574	0.72363772
C	-4.47457706	0.00141284	0.74544989
H	-5.51744317	0.00157166	1.04568682
C	-3.78055102	-1.19655524	0.56120031
H	-4.27463657	-2.14854353	0.73263033
C	-2.43992279	-1.20373301	0.16830180
H	-1.94160992	-2.15886714	0.07918867
C	0.40219799	1.19818915	-0.42120121
C	0.01163364	2.33752884	-1.14650531
H	-0.86058474	2.29379078	-1.78903273
C	0.76605758	3.50727375	-1.07311036
H	0.45787864	4.37206864	-1.65277639
C	1.92566889	3.56775381	-0.28314318
H	2.50528496	4.48370597	-0.23183525
C	2.34511625	2.43016075	0.39593208
H	3.26320246	2.42374577	0.97508154
C	1.60340743	1.23663922	0.32477508

Table S7. Optimized S_1 geometry of compound **1** at the TPSSh/6-31+G(d,p) level of theory (Å).

Atom	X	Y	Z
O	2.58720073	0.00297713	2.15799910
C	1.80159877	0.00203956	1.15698759
C	1.43555109	-1.23697906	0.45104651
C	2.12845851	-2.45335067	0.62037845
H	2.85447107	-2.52660787	1.42391356
C	1.90012860	-3.52897230	-0.24556710
H	2.45071358	-4.45446604	-0.10181597
C	0.98717648	-3.42516939	-1.30293052
H	0.82450921	-4.25813654	-1.97866034
C	0.24093051	-2.23969824	-1.45901670
H	-0.50741929	-2.14885117	-2.24064577
C	0.44005625	-1.20771141	-0.55696321
N	-0.36833649	-0.00058290	-0.53728741
C	-1.65949559	-0.00199810	-0.09306181
C	-2.35176519	1.23101451	0.13891170
H	-1.83836367	2.17017211	-0.01688039
C	-3.66440851	1.21431324	0.57060570
H	-4.17893576	2.15262051	0.74632095
C	-4.33485448	-0.00463583	0.78682570
H	-5.36612034	-0.00565019	1.12158886
C	-3.66185096	-1.22226205	0.57111327
H	-4.17440916	-2.16157445	0.74721781
C	-2.34917132	-1.23638273	0.13942723
H	-1.83381782	-2.17452903	-0.01594455
C	0.43711826	1.20849105	-0.55695772
C	0.23532584	2.24004619	-1.45890429
H	-0.51291215	2.14741095	-2.24042999
C	0.97868650	3.42732980	-1.30283461
H	0.81389685	4.25993608	-1.97849468
C	1.89151922	3.53330195	-0.24558107
H	2.43985266	4.46013419	-0.10184719
C	2.12255481	2.45821627	0.62031611
H	2.84847599	2.53323180	1.42377796
C	1.43257593	1.24016937	0.45102457

Table S8. Optimized T_1 geometry of compound **1** at the TPSSh/6-31+G(d,p) level of theory (Å).

Atom	X	Y	Z
O	3.07515631	-0.00049083	1.80154224
C	2.09655476	-0.00031709	0.97680656
C	1.58647137	-1.22626189	0.36892978
C	2.28184393	-2.45409182	0.43972395
H	3.15664544	-2.50630419	1.07977785
C	1.88168446	-3.55050040	-0.32241094
H	2.44604598	-4.47689316	-0.26335866
C	0.77907647	-3.46367587	-1.19070336
H	0.49442531	-4.30616716	-1.81170056
C	0.03344895	-2.27934227	-1.23653561
H	-0.82836090	-2.19355293	-1.89094929
C	0.40749561	-1.20435262	-0.42907935
N	-0.37448646	0.00009930	-0.34553631
C	-1.71090886	0.00026656	0.01161224
C	-2.41069719	1.22672444	0.22457001
H	-1.88650774	2.16935699	0.15539671
C	-3.75588362	1.21385553	0.55460848
H	-4.26988475	2.15555499	0.71409291
C	-4.44809549	0.00054921	0.70496552
H	-5.50102497	0.00065909	0.96453749
C	-3.75609028	-1.21289868	0.55479490
H	-4.27024605	-2.15448640	0.71444025
C	-2.41090850	-1.22604231	0.22475384
H	-1.88686599	-2.16877029	0.15572845
C	0.40788437	1.20431805	-0.42904214
C	0.03425893	2.27943239	-1.23652348
H	-0.82751403	2.19393841	-1.89102301
C	0.78027934	3.46351959	-1.19063460
H	0.49594346	4.30610703	-1.81164615
C	1.88286561	3.54997172	-0.32227983
H	2.44753037	4.47617703	-0.26318548
C	2.28262723	2.45341448	0.43984577
H	3.15743457	2.50531045	1.07991777
C	1.58684857	1.22581459	0.36899625

References

1. Frisch G. W.; Schlegel, H. B.; Scuseria, G. E.; Robb, M. A.; Cheeseman, J. R.; Scalmani, G.; Barone, V.; Petersson, G. A.; Nakatsuji, H.; Li, X.; Caricato, M.; Marenich, A. V.; Bloino, J.; Janesko, B. G.; Gomperts, R.; Mennucci, B.; Hratch, D. J., M. J. . T. Gaussian 16, Rev. A.03. *Gaussian, Inc., Wallingford, CT* **2016**.
2. F. Neese, F. Wennmohs, U. Becker and C. Riplinger, *J. Chem. Phys.*, 2020, **152**, 224108.
3. F. Neese, *WIREs Comput. Mol. Sci.*, 2022, **12**, e1606.
4. T. Lu and F. Chen, *J. Comput. Chem.*, 2012, **33**, 580–592.
5. Z. Liu, T. Lu and Q. Chen, *Carbon*, 2020, **165**, 461–467.
6. W. Humphrey, A. Dalke and K. Schulten, *J. Mol. Graphics*, 1996, **14**, 33–38.
7. K. Shizu and H. Kaji, *Commun. Chem.*, 2022, **5**, 1–6.
8. J.-L. Brédas, D. Beljonne, V. Coropceanu and J. Cornil, *Chem. Rev.*, 2004, **104**, 4971–5004.
9. Y. Olivier, B. Yurash, L. Muccioli, G. D'Avino, O. Mikhnenko, J. C. Sancho-García, C. Adachi, T.-Q. Nguyen and D. Beljonne, *Phys. Rev. Mater.*, 2017, **1**, 075602.